Utility of integrated IMERG precipitation and GLEAM potential evapotranspiration products for drought monitoring over mainland China

Shanhu Jiang[a,b], Linyong Wei[b], Liliang Ren[a,b*], Chong-Yu Xu[c], Feng Zhong[b], Menghao Wang[b], Linqi Zhang[b], Fei Yuan[a] and Yi Liu[b]

[a]*State Key Laboratory of Hydrology-Water Resources and Hydraulic Engineering, Hohai University, Nanjing 210098, China*

[b]*College of Hydrology and Water Resources, Hohai University, Nanjing 210098, China*

[c]*Department of Geosciences, University of Oslo, N-0316 Oslo 1047 Blindern, Norway*

Revised and resubmitted to *Atmospheric Research*

*Corresponding author:

Professor Liliang Ren

Hohai University, Nanjing 210098, China

Email: njRLL9999@126.com

ABSTRACT

In this paper, we comprehensively evaluated the utility of integrated long-term satellite-based precipitation and evapotranspiration products for drought monitoring over mainland China. The latest Integrated Multi-satelliteE Retrievals for Global Precipitation Measurement V06 three Runs precipitation products, i.e., the near real-time Early Run (IMERG-E) and Late Run (IMERG-L) and the post-real time Final Run (IMERG-F), and the Global Land Evaporation Amsterdam Model V3.3a (GLEAM) potential evapotranspiration (PET) products from 2001 to 2017 were considered. The accuracy of IMERG precipitation and GLEAM PET products was first evaluated against observed precipitation and Penman-Monteith method estimated PET, respectively, based on dense meteorological station network. The Standard Precipitation Evapotranspiration Index (SPEI) calculated based on IMERG precipitation and GLEAM PET products (SPEIs, including $SPEI_E$, $SPEI_L$ and $SPEI_F$ corresponding to IMERG-E, IMERG-L and IMERG-F, respectively) were then validated by using SPEI calculated based on meteorological data (SPEIm) at multiple temporal-spatial scales. Finally, four typical drought events were selected to analyse the ability of SPEIs to characterize the temporal-spatial evolution of drought situations. The results showed that the IMERG-F presents much better performance than IMERG-E and IMERG-L in terms of higher CC and smaller BIAS and RMSE values over mainland China. The GLEAM PET well simulated the change trend of reference PET, but generally underestimated reference PET in Northwest China (NW), Xinjiang (XJ) and Qinghai–Tibet plateau (TP). In general, the performances of SPEIs over eastern China and Southwest China (SW) were significantly superior to their performances in the NW, XJ, and TP regions. Even though the $SPEI_F$ performed the best, the $SPEI_E$ and $SPEI_L$ also performed reasonably well in some specific regions. SPEIs can well capture the temporal process and reasonably reflect the spatial characteristics for four typical drought events. It is thus highlighted that the latest IMERG precipitation (especially for IMERG-F) and GLEAM PET products could be used as alternative data sources for comprehensive drought monitoring, on account of the water balance principle over mainland China, particularly in eastern China and SW China. The outcomes of this study will provide valuable references for drought monitoring by integration of multi-source remote-sensing datasets in the GPM era.

Keywords: IMERG; GLEAM; Standardized Precipitation Evapotranspiration Index (SPEI); Drought monitoring; Mainland China

1 Introduction

Drought is a kind of natural disaster with long duration, wide influence and strong destructiveness that can seriously affect human life, agricultural production, economic growth and ecological environment (Sheffield et al., 2012; AghaKouchak et al., 2015; Jiang et al., 2019). With the effects of global climate warming and intensive human activities, the severity, duration and effect of droughts are further aggravated (Dai, 2011; Trenberth et al., 2014; Wang et al., 2017a). Accurate and timely drought monitoring can provide crucial scientific basis for drought disasters preventing and mitigating (Sahoo et al., 2015; Bayissa et al., 2017). Hence, it is urgent to quantitatively monitor drought in term of its occurrence, development, affected area, and intensity by developing more effective drought monitoring tools and utilizing more accurate datasets (Sandholt et al., 2002; West et al., 2019; Li et al., 2020).

Being aimed at different types of drought (i.e., meteorological, agricultural, hydrological and socioeconomic droughts), corresponding drought indices are developed to monitor drought at different temporal-spatial scales (Mishra and Singh, 2010; Lloyd-Hughes, 2014). For example, Standardized Runoff Index (SRI) is used for monitoring hydrological drought (Shukla and Wood, 2008). Crop Water Deficit Index (CWDI) is used for assessment of agricultural drought (Moran et al., 1994). Socioeconomic Drought Index (SEDI) is used to analysis socioeconomic drought (Mishra and Singh, 2010). For meteorological drought, the Standardized Precipitation Index (SPI) (McKee et al., 1993), the Palmer Drought Severity Index (PDSI) (Palmer, 1965) and the Standardized Precipitation Evapotranspiration Index (SPEI) (Vicente-Serrano et al., 2010) are the three widely used drought indices. SPI is often used because it has simple calculation process, low data requirements (only precipitation), and flexible timescales. However, SPI has an inherent limitation that it does not consider the evapotranspiration factor. Although the main cause of meteorological drought is precipitation anomalies over a period of time, under the condition of a complex underlying surface, evapotranspiration is also an important impact factor (Begueria et al., 2014). The PDSI comprehensively analyses drought from the perspective of precipitation, evapotranspiration, and runoff, and thus it is a popular for studying climate change (Dai, 2011). However, PDSI has some inherent limitations, for instance complex data requirements, fixed time scales and weak spatial comparability (Vicente-Serrano et al., 2011). SPEI inherits the advantages of SPI and PDSI to consider both precipitation and evapotranspiration, and uses the simple calculation method adopted by SPI. Since its development, SPEI has become one of the more comprehensive monitoring methods, and it has been widely used in meteorological drought research (Yu et al., 2014; Begueria et al., 2014). In this study, we will focus on meteorological drought.

Traditionally, the variables (i.e., precipitation, evapotranspiration, and so on) used to calculate meteorological drought indices are usually obtained from in-situ meteorological station measurements (Jiang et al., 2012; AghaKouchak et al., 2015). However, precipitation and evapotranspiration data are often difficult to be continuously and accurately observed in many regions where meteorological stations are limited (Wang et al., 2017b; Duan et al., 2019; Jiang et al., 2020). In a large-scale space, there are some inaccuracies in drought monitoring based on limited station observations. In addition, measurements from meteorological and rainfall stations are usually difficult to retrieve for many reasons, for instance data-sharing policies. Towards the 20th century, with the continuous development of the aerospace industry and satellite remote-sensing technology, numerous satellite precipitation products (SPPs) were operationally available. In the Tropical Rainfall Measuring Mission (TRMM) era, the widely used SPPs include the TMPA (Huffman et al., 2007), CMORPH (Joyce et al., 2004), PERSIANN (Sorooshian et al., 2000) and CHIRPS (Funk et al., 2015). As the successor of the TMPA, the Integrated Multi-satellitE Retrievals for Global Precipitation Measurement (IMERG) has the advantages of larger coverage, higher spatiotemporal resolution and more accurate rainfall estimations (Hou et al., 2014; Huffman et al., 2015; Jiang et al., 2018). IMERG has released data with four official versions; and the latest Version 06 (V06) products were released in May, 2019. Compared to previous versions, IMERG V06 introduced several major changes, i.e., improvement to the parent GPM products, modification of the satellite inter-calibrations, inclusion of additional sensors and refinement of the Kalman filter process (Huffman, et al., 2019). The retrospective processed IMERG V06 created a homogeneous record starting from 2000 (and eventually from 1998) of the TRMM era and extended coverage to the poles, aiming to replace the widely used TMPA datasets for operational and research applications (Tan, 2019). The longer period coverage of the

IMERG V06 makes it with greater application utility in hydrometeorological field, such as drought monitoring (Tang et al., 2020). As with SPPs, there also have some satellite evapotranspiration products were available, for instance the Moderate Resolution Imaging Spectroradiometer (MODIS) i.e., MOD16 evapotranspiration data with different temporal and spatial resolutions (Mu et al., 2007, 2011); the coupled diagnostic biophysical model (PML-V2), estimation of 500m and 8-day resolution global evapotranspiration for 2000-2017 (Zhang et al., 2019). The Global Land Evaporation and Amsterdam Model (GLEAM) is a set of algorithms that separately estimate the different components of evapotranspiration based on multi-satellite observations (Miralles et al., 2011). Compared to MOD16 and PML-V2 data, GLEAM products have a longer time series (from 1980 to date) and relatively better accuracy globally (Martens et al., 2017). Meanwhile, MOD16 products cannot obtain evapotranspiration data in most deserts, including the Gobi Desert of western China. The long-term GLEAM evapotranspiration products thus have great potential utility for drought monitoring (Vicente-Serrano et al., 2018; Zhao and Ma, 2019; Peng et al., 2020a).

There have been some attempts to comprehensively evaluate the drought monitoring ability of high-resolution SPPs on different temporal-spatial scales (Sahoo et al., 2015; Guo et al., 2016; Zambrano et al., 2017; Bayissa et al., 2017; Agutu et al. 2017; Jiang et al., 2017; Lu et al., 2018; Xu et al., 2019; Chen et al., 2020). For instance, Sahoo et al. (2015) found that TMPA research products (i.e., TMPA 3B42V6 and 3B42V7) performed satisfactorily in monitoring large-scale drought events with short-term data records. Guo et al. (2016), Lu et al. (2018), and Xu et al. (2019) found that PERSIANN-CDR, CMORPH-BLD and MSWEP V2.1 were useful for drought monitoring in eastern China. Zambrano et al. (2017), Bayissa et al. (2017), and Agutu et al. (2017) found that CHIRPS performed well in drought monitoring in Chile, Ethiopia, and East Africa, respectively.

However, the drought monitoring utility of the newly released longer-period IMERG V06 is still unclear. Also, these studies just used the SPI index, without considering the evapotranspiration influence. Some recent studies have begun to consider evapotranspiration, for example Zhong et al. (2019) and Bai et al. (2020) adopted the PDSI and SPEI to evaluate the drought monitoring utility of SPPs with considering evapotranspiration. However, in both of these studies, the potential evapotranspiration (PET) data for calculating PDSI and SPEI were based on meteorological station data, without using the recently developed remote-sensing evapotranspiration products. Based on GLEAM actual evapotranspiration and GLEAM atmospheric evaporative demand (i.e., the PET) data, Vicente-Serrano et al. (2018) highlighted the fact that GLEAM evapotranspiration data have good drought monitoring potential across a wide range of regions. On account of open-access satellite precipitation and satellite evapotranspiration products, integrated use of the two products to monitor drought characteristics is a new technical method that deserves to be more fully investigated (West et al., 2019; Chawla et al., 2020). Hence, it is urgent to study the utility of the newly released SPPs and remote-sensing evapotranspiration datasets for more effective drought monitoring.

Therefore, the purpose of this study was to analyse the precision characteristics of the latest IMERG V06 three Runs precipitation and GLEAM V3.3 PET products and to evaluate their drought monitoring utility over mainland China. First, the precision characteristics of IMERG precipitation and GLEAM PET products were evaluated against observed precipitation and estimated PET data, respectively. Then, the SPEI based on IMERG precipitation and GLEAM PET products, i.e., SPEIs, were validated by using SPEIm (SPEI calculated based on meteorological data) at multiple temporal-spatial scales. Finally, four typical drought events were selected to analyse the ability of the SPEIs to characterize the temporal-spatial evolution of drought situations. The outcomes of this study will provide a valuable reference for drought monitoring by integrating multi-source remote-sensing datasets in GPM era.

2 Study area and data

2.1 Study area

Mainland China (Fig. 1) has a complex topography and diverse climatic conditions. The elevation can be roughly divided into three categories from west to east: over 3000 m, 1000−3000 m and lower than 1000 m a.m.s.l. For the evaluation at different regional scales, we followed Chen et al. (2013) to divide mainland China into eight regions, depending on the distribution of precipitation, mountain range and altitude. They are Northeast China (NE), Northern China (NC), the middle and lower reaches of the Yangtze River (CJ), Southeast China (SE), Northwest China (NW), Southwest China (SW), Xinjiang (XJ) and the Qinghai–Tibet plateau (TP), excluding Taiwan (Lu et al., 2019). Among these regions, TP is mainly dominated by a plateau mountain climate. SW, SE and CJ are governed by a subtropical monsoon climate. NE and NC belong to a temperate monsoon climate. NW and XJ are affected by an arid or semi-arid climate. In the study, NE, NC, CJ and SE belonged to eastern China, and SW, NW, XJ and TP belonged to western China. The spatial distribution density of meteorological stations is declining from eastern China to western China.

Insert Figure 1 about here

2.2 Satellite precipitation and evapotranspiration datasets

IMERG is a new-generation precipitation product that provides estimates of precipitation on a 0.1° × 0.1° grid within 90°N/S every half-hour (Hou et al., 2014).

Compared with TMPA precipitation products, IMERG can capture micro and solid precipitation more accurately. IMERG has released data with four official versions; the Version 06 (V06) algorithm was recently upgraded in May 2019. IMERG V06 has retrospectively processed IMERG to the TRMM era to create a homogeneous record starting from 1998, aiming to replace the widely used TMPA datasets. IMERG V06 provides three Runs to accommodate different user requirements for latency and accuracy, including the near real-time Early Run (released 4 hr after real-time, hereafter called IMERG-E) and Late Run (released 12 hr after real time, hereafter called IMERG-L), and the post real-time Final Run (delayed about 3.5 month, hereafter called IMERG-F) IMERG product (Huffman, et al., 2019). As the upgraded successor of TRMM, several studies have found that the V06 IMERG-F product outperforms TMPA 3B42V7, CMORPH, PERSIANN-CDR, CHIRPS and some other SPPs at daily and hourly time scales over mainland China (Tang et al., 2020; Yu et al., 2020). However, the monthly scale precision characteristics of the retrospective V06 IMERG three Runs products over mainland China are still unclear (Peng et al., 2020b). Thus, it is necessary to explore the drought monitoring utility of the latest long-term V06 IMERG three Runs products over large regions, like mainland China. In this study, the latest V06 IMERG-E, IMERG-L and IMERG-F daily precipitation products from 2001 to 2017 were used, and the data were further accumulated into monthly values for drought monitoring.

GLEAM contains all composition data of evapotranspiration, such as actual evaporation (AET), potential evapotranspiration (PET), evaporative stress factor, root-zone soil moisture, surface soil moisture and so on (Miralles et al., 2011). The

GLEAM PET dataset was retrieved from the Priestley–Taylor formula based on surface radiation and near-surface air temperature from multiple reanalysis datasets. In May 2019, the latest version 3.3 (V3.3) GLEAM evapotranspiration datasets were produced, with multiple time resolutions (day, month and year) and 0.25° spatial resolution for the years from 1980 to 2018. Since their development, GLEAM evapotranspiration products have been widely used in the hydrometeorology fields (Vicente-Serrano et al., 2018). In this study, the monthly GLEAM V3.3a PET data from 2001 to 2017 were used.

2.3 In-situ observation datasets

The daily China surface climate dataset Version 3.0 released by the National Meteorological Data Center was used. The data resource takes observation data from national meteorological stations. The uniformity of the dataset was tested using the quality control mean and the RclimDex software package, including checking the spatiotemporal and internal consistency of the data to ensure the data quality is effectively guaranteed (Shen et al., 2010). This dataset is often used as benchmark data to evaluate the accuracy of SPPs over mainland China (Zhong et al., 2019). In this study, meteorological data from 2001 to 2017 with relatively complete time series from 807 meteorological stations (Fig. 1) were selected. The daily PET, which is used as benchmark evaporation data, was calculated by using the Penman–Monteith model recommended by Food and Agriculture Organization (Allen et al., 1998). The daily PET and precipitation data of each station were accumulated into monthly values.

In this study, the nearest grid-to-point matching method (Chen et al., 2018) was used to extract the corresponding IMERG precipitation and GLEAM PET data in terms of the longitude and latitude coordinates of the 807 meteorological stations. The regional average values were calculated based on a subset of pixels corresponding to meteorological stations within each sub-region.

3 Methodology

3.1 Standardized Precipitation Evapotranspiration Index

SPEI inherited the calculation method of SPI and considers the influence of evapotranspiration on drought under changing environments. Calculation of SPEI is roughly divided into three steps. First, the difference between the monthly precipitation and PET, i.e., the D value, is calculated as input. Then, the D value series are fitted with a log-logistic distribution. Finally, the D value series are transformed into quantiles to get the SPEI values. The specific calculation formula of SPEI is available in the literature (Vicente-Serrano et al., 2010). The drought ranking of SPEI is shown in Table 1. In this study, the SPEI calculated based on IMERG precipitation and GLEAM PET products are abbreviated as SPEIs (including, $SPEI_E$ calculated based on IMERG-E precipitation and GLEAM PET, $SPEI_L$ calculated based on IMERG-L precipitation and GLEAM PET, and $SPEI_F$ calculated based on IMERG-F precipitation and GLEAM PET) and the SPEI calculated based on meteorological data is abbreviated as SPEIm.

Insert Table 1 about here

3.2 Statistical metrics

Six commonly used statistical indicators were adopted. The correlation coefficient (CC), which expresses the degree of linear correlation (consistency) between the evaluation data against the reference data; relative bias (BIAS), which reflects the deviation degree between the evaluation data against the reference data; root mean square error (RMSE), which shows the dispersion degree between the evaluation data against the benchmark data; mean error (ME), which indicates the overall level of evaluation data error; probability of detection (POD) and false alarm rate (FAR) refer to the hit rate and false alarm rate of the evaluated data in capturing drought events, respectively. First, CC, BIAS, RMSE and ME were selected to evaluate the error characteristics of IMERG precipitation and GLEAM PET on a monthly scale. Then, CC, RMSE, POD and FAR were used to evaluate the precision of SPEIs. The calculation formulas of the above indicators are as follows:

$$CC = \frac{\sum_{i=1}^{n}\left(G_i - \overline{G}\right)\left(S_i - \overline{S}\right)}{\sqrt{\sum_{i=1}^{n}\left(G_i - \overline{G}\right)^2}\sqrt{\sum_{i=1}^{n}\left(S_i - \overline{S}\right)^2}} \tag{1}$$

$$BIAS = \frac{\sum_{i=1}^{n}(S_i - G_i)}{\sum_{i=1}^{n} G_i} \times 100\% \tag{2}$$

$$RMSE = \sqrt{\frac{1}{n}\sum_{i=1}^{n}\left(S_i - G_i\right)^2} \tag{3}$$

$$ME = \frac{1}{n}\sum_{i=1}^{n}\left(S_i - G_i\right) \tag{4}$$

$$POD = \frac{H}{H + M} \tag{5}$$

$$FAR = \frac{F}{H + F} \tag{6}$$

where n is the total number of months, referring to the length of evaluation data in time series; S_i is the evaluation data; G_i is the reference data; H is the number of droughts that occurred and were correctly monitored by SPEIs; M is the number of droughts that occurred and were not monitored by SPEIs; F is the number of droughts that did not actually occur but were monitored by SPEIs.

4 Results

4.1 Evaluating the accuracy of IMERG precipitation and GLEAM PET

Fig. 2 shows the spatial distribution of CC, BIAS and RMSE for the daily IMERG precipitation products versus gauge observations for 2001−2017. Fig. 3 is similar to Fig. 2, but for monthly time scale. For spatial precision patterns, it can be seen that the precision distribution of IMERG precipitation products for both daily and monthly time scales are identical. The performance of CC and BIAS declined from southeast to northwest. While due to the precipitation intensity distribution, the RMSE values in southeast China are relatively high. For temporal precision characters, we can see that the IMERG precipitation products have much better performance at monthly time scale than that of daily time scale in terms of higher CC and better RMSE values as the temporal scale enlarges, especially for the IMERG-F product. For different IMERG Run products performances, the two near real-time IMERG-E and IMERG-L products demonstrate comparable performances both at daily and monthly time scales. The IMERG-F presents much better performance than IMERG-E and IMERG-L in terms of higher CC values and smaller BIAS and RMSE values, due to bias adjusted using monthly precipitation data of the Global Precipitation Climatology Centre (GPCC).

Table 2 lists the quantiles (5%, 50% and 95%) of statistical indicators at a grid/station scale in the eight study regions for the monthly IMERG precipitation products. The IMERG-F product demonstrates the best performance among the three SPPs, which has high consistency (with average CC of 0.92), small deviation (with average BIAS of 10%) and low error (with average RMSE of 26.42 mm/month) in most parts of mainland China.

The IMERG-E and IMERG-L products show acceptable performances, which have relatively high consistency (with average CC of 0.80 and 0.81, respectively), small deviation (with average BIAS of 13.54% and 13.5%, respectively) and relatively large error (with average RMSE of 46.48 and 46.68 mm/month, respectively). More specifically, the CC values of IMERG precipitation products are lower in some areas of XJ and TP where there are complex terrain, dry climate and few meteorological stations, but somewhat higher in eastern China, which has humid climate and high density of meteorological stations. The most BIAS values in eastern China were in the range of −10% to 20%, while prominently higher or lower than the reference data in the western China. The RMSE value decreased with decreasing precipitation from SE to XJ. These results indicate that complex terrain and dry climate affect the accuracy of IMERG precipitation products. Additionally, the less in-situ gauge data for satellite precipitation error correction and the algorithm of satellite precipitation inversion may also affect the accuracy of IMERG (Guo et al., 2016). IMERG-F uses GPCC data for correction to reduce deviation, but meteorological stations of GPCC in western China are relatively sparse, and hence, it is difficult to ensure the reliability of deviation correction about the satellite product (Wei et al., 2019). Generally, IMERG precipitation products, especially for the IMERG-F product, have reliability and high precision in eastern China, SW and NW but they show relatively poorer precision in XJ and TP.

Insert Figure 2 about here

Insert Figure 3 about here

Insert Table 2 about here

Fig. 4 shows the spatial distribution of the CC, BIAS and RMSE between GLEAM PET against reference PET at daily and monthly time scales over mainland China. We can see that the daily and monthly spatial precision patterns of GLEAM PET are identical. As the temporal scale enlarges, the GLEAM PET demonstrates much better performance at monthly time scale than that of daily time scale in terms of higher CC and better RMSE values. For monthly time scale, the CC is relatively high for most grids of mainland China (with CC larger than 0.88), especially in eastern China and XJ. Even in the northern TP and in most parts of SW, the CC values were in the range of 0.73 to 0.88. These results show that GLEAM PET can simulate the PET trend very well over mainland China. However, the difference of BIAS values between the eastern and western China is obvious. The BIAS values in most eastern China areas were in a range of −20% to 20%, whereas the negative BIAS values in western China were large, which indicate that GLEAM underestimated the reference PET in western China. This is more apparent in Table 2, for example, the 5%, 50%, and 95% BIAS and ME were less than 0 in some regions except CJ, SE and SW. This may be related to the different calculation methods of reference PET data and the GLEAM model and different input data. In addition, the net radiation data appear negative value in winter and as an input to GLEAM model. Thus, the value of PET output appears negative in some areas (Martens et al., 2018). The RMSE values were lower than 30 mm/month in most areas of eastern China, whereas there were higher RMSE values and greater variation among the different meteorological stations in western China. The absolute values of BIAS and RMSE all increased from the SE with humid climate to the western China with dry climate. Overall, GLEAM had a high correlation with reference PET data over mainland China but a systematic deviation and error, especially in NW, XJ and TP.

Insert Figure 4 about here

The Quantile−Quantile (Q−Q) plot can directly evaluate the applicability and deviation between the satellite product and reference data for different quantiles (Gao et al., 2017; Zhong et al., 2019). Fig. 5 shows the Q–Q plot of the regional averaged IMERG precipitation and GLEAM PET for the eight regions, expressing as log-log coordinates for convenient analysis of low values. It can be intuitively seen that IMERG has good applicability in all regions (except for XJ) for precipitation above 100 mm. Precipitation within 10−100 mm is estimated to be low in SE and SW, which have high precipitation, and in TP which has high altitude (Guo et al., 2016). Precipitation with less than 10 mm, the value estimated was slightly higher in NE and NC, whereas it was more obviously low in SE, SW, XJ and TP. These results are consistent with Fig. 3. For the PET dataset, it can be intuitively seen that GLEAM underestimated the reference PET data over mainland China; it was especially relatively low with regard to different magnitudes in NW and XJ. However, in the relatively humid CJ, SE and SW regions, the ability of PET estimated by GLEAM was better than that in other regions. These results are consistent with Fig. 4. IMERG precipitation products and GLEAM PET all performed worse in XJ and TP regions. Thus, because of the constraints of geography, climate and satellite inversion algorithms, the accuracy of satellite products does not guarantee reliability in regions with sparse in-situ stations, dry climate and complex terrain in China.

Insert Figure 5 about here

4.3 Evaluation the accuracy of satellite-based SPEI at grid scale

Fig. 6 shows the spatial distribution of statistical indicators by SPEIs (i.e., $SPEI_E$, $SPEI_L$ and $SPEI_F$) at 3-month timescale over mainland China. Table 3 lists 5%, 50% and 95% values of statistical indicators about SPEIs at 3-month timescale. Over mainland China, the average CC, RMSE, POD and FAR values were 0.60, 0.92, 0.61 and 0.39 between $SPEI_E$ against SPEIm, respectively, 0.61, 0.90, 0.62 and 0.38 between $SPEI_L$ against SPEIm, respectively, and 0.78, 0.67, 0.74 and 0.26, between $SPEI_F$ against SPEIm, respectively. We can see that the performance of $SPEI_E$, $SPEI_L$ and $SPEI_F$ varies greatly; the $SPEI_F$ takes much better performance than $SPEI_L$ and $SPEI_F$ in each region and MC. In additional, from the four statistical indicators in Fig. 6, the precision of SPEIs increased gradually from west to east. The SPEIs all performed best in eastern China and Southwest China, particularly for the CJ and SE regions; the NC region took second place. However, SPEIs showed the worst performance in the XJ and TP regions. Moreover, compared with eastern China, the values of statistical indicators at different grids in western China (specifically of the XJ and TP regions) were quite different, indicating the poor drought monitoring utility of SPEIs in western China, which may be related to the performance of satellite products and the local complex climate and geographical conditions. In a word, $SPEI_F$ demonstrated good utility in drought monitoring over mainland China, which performed best in eastern China and SW, followed by NW, and it performed worst in XJ and TP (Zhong et al., 2019; Bai et al., 2020). $SPEI_L$ and $SPEI_F$ show good performance in CJ, SE, and SW regions. It should be noted that in all regions of China, the drought monitoring results of $SPEI_E$ and $SPEI_L$ might have much more uncertainties than $SPEI_F$

result.

Insert Figure 6 about here

Insert Table 3 about here

4.2 Evaluation the accuracy of satellite-based SPEI at regional scale

For further evaluating the drought monitoring utility of IMERG precipitation and GLEAM PET at regional scale over mainland China, Fig. 7 displays the statistical indicators (CC, RMSE, POD and FAR) of regional average SPEIs (i.e., $SPEI_E$, $SPEI_L$ and $SPEI_F$) against SPEIm at 3-month timescale in the eight regions. Generally, the $SPEI_F$ demonstrates much better performance than $SPEI_L$ and $SPEI_F$ in each region. We can see that $SPEI_F$ agrees well with the SPEIm over mainland China, except for the XJ and TP regions. The CC values were higher than 0.94 in eastern China and between 0.77 and 0.96 in western China. The RMSE values were between 0.11 and 0.30, which are characterized by small values (smaller than 0.23) in the eastern China and SW regions. $SPEI_F$ could detect drought events much better in eastern China and SW (with POD values larger than 0.77), followed by NW and XJ, with the worst performance in TP. The FAR value was no more than 0.34 in each region, which demonstrates a lower false alarm for monitoring drought by satellite datasets. Meanwhile, the $SPEI_L$ and $SPEI_F$ show good performance in CJ, SE, and SW regions, with CC values of higher than 0.83 and RMSE values of smaller than 0.35; and they demonstrate relative acceptable performance in NE and NC, with CC values of higher than 0.74 and RMSE values of 0.47; whereas they demonstrate poor performance in NW, XJ and TP.

Insert Figure 7 about here

Fig. 8 exhibits the scatter plots of grid averaged SPEIs (i.e., $SPEI_E$, $SPEI_L$ and $SPEI_F$) against SPEIm at 3-month timescale for eight regions during 2001–2017. The terms re, rl and rf represent the slope of the linear fit between $SPEI_E$ against SPEIm, $SPEI_L$ against SPEIm and $SPEI_F$ against SPEIm, respectively. It can be seen that in the humid CJ, coastal SE and mountainous SW, the consistencies between SPEIs and SPEIm were the best, and the values are distributed evenly and thinly on the line (r is close to 1). In the NE with cold weather and heavy snowfall in winter and NC with a plain landform, SPEIs better estimated the drought intensity (r is between 0.68–1.02). In arid or semi-arid NW and XJ, and high latitude TP, the SPEIs underestimated the values of SPEIm dramatically, with r in the range of 0.55–0.86. In general, similar to the results of Fig. 7, the $SPEI_F$ shows satisfactory performance in most regions in mainland China (except for XJ and TP). The $SPEI_E$ and $SPEI_L$ demonstrate good performance in CJ, SE, and SW.

Insert Figure 8 about here

4.4 Validation analysis of several typical drought events

In order to further validate and analyse the performance of SPEIs in reflecting the spatiotemporal variation of drought events, in terms of the SPEIs performance from multiple angles and the previous assessment results, we selected four typical regions for specific case studies: NE, NC, CJ and SW. The NC and SW were selected to analyse two widespread drought events, i.e., the prolonged drought disaster from 2010 to 2011 in NC (Xu et al., 2019) and the severe drought disaster from 2009 to 2010 in SW (Zhang et al., 2013). The NE was selected because it is an important food production base of China. The CJ was selected for its abundant water resources and its importance as an agricultural base in China. The drought events from December 2001 to November 2002, in NE (Zhong et al., 2019) and from March 2011 to September 2011, in CJ (Chen et al., 2020) were selected as typical drought events for NE and CJ, respectively. The drought duration, drought severity and drought intensity information are shown in Table 4.

Insert Table 4 about here

Fig. 9 shows the grid averaged SPEIs against SPEIm during 2001–2017 and the ratio of drought stations (RDS), i.e., the number of meteorological stations with drought to the total number of meteorological stations for the four specific case study regions. A higher RDS means a wider area covered by drought, which can be used to reflect the ratio of drought area to some extent. There is a consistent relationship between SPEI and RDS on drought events for different time series, i.e., a smaller value of SPEI in accord with a larger value of RDS and a larger value of SPEI in accord with a smaller value of RDS. The duration of a typical drought event presented in Table 4 is plotted on the corresponding subgraph in Fig. 9, represented by the area with grey background, which involves the lowest value of SPEI and the highest value of RDS in succession. In general, although SPEIs have some small deviations in simulating the values of SPEIm and the drought area ratio, they can well capture the evolution of drought events. For example, the drought simulation performance by SPEIs are very accurate in NE, CJ and SW. The matching degree of SPEIs and SPEIm are slightly weak in NC, whereas $SPEI_F$ can still identify the start–end time and severity of a typical drought event.

Insert Figure 9 about here

Fig. 10 shows the spatial pattern of a typical drought event with the lowest regional SPEI value and the largest RDS value for a specific month (i.e., Fig. 9 and Table 4) for the four selected regions. The spatial distribution characteristics of SPEIs are highly consistent with the results of SPEIm in each region; there are only some small differences regarding drought severity and the drought centre in the local area. For example, the spatial distributions of SPEIs are highly consistent with the SPEIm in March 2002, in NE, and in February 2010, in SW, whereas the drought severities estimated by SPEIs are lower than that of the benchmark drought. In CJ, the drought severity monitored by $SPEI_F$ is slightly higher than the situation of SPEIm. In NC, the drought severities monitored by $SPEI_E$ and $SPEI_L$ are obviously lower than the situation of SPEIm. On the whole, the accuracy of satellite-derived SPEIs (especially for $SPEI_F$) are acceptable for simulating typical drought events of the four selected regions, indicating that the IMERG precipitation (especially for IMERG-F precipitation) and GLEAM PET are useful in detecting the timing, intensity and magnitude of drought events.

Insert Figure 10 about here

5 Discussion

5.1 Uncertainties of SPEIs based on IMERG precipitation and GLEAM PET data

In the era of remote-sensing big data, high-precision satellite precipitation datasets and evapotranspiration datasets are continuously derived and updated (West et al., 2019). To reduce the impact of errors of remote-sensing precipitation on SPEIs, it is necessary to consider and select the best performing satellite precipitation and evapotranspiration products for drought monitoring. For the post real-time research-quality IMERG-F product, Tang et al. (2020) and Yu et al. (2020) highlighted that the V06 IMERG-F product is superior to other datasets, i.e., nine satellite and reanalysis precipitation datasets, at daily and hourly time scales in China. According to some other previous statistical evaluations, the IMERG-F precipitation had high consistency, small deviation and low error compared to other commonly used SPPs (i.e., TMPA 3B42, CMORPH, PERSIANN-CDR, CHIRPS, and so on) in most parts of mainland China (Wang et al., 2018; Yuan et al., 2018). In addition, the monthly-scale V06 IMERG-F product adjusted by GPCC data has good performance in terms of estimating drought occurrence and development at the monthly and seasonal time scales (Peng et al., 2020b). Thus, the new-generation V06 IMERG-F precipitation product has good potential for drought monitoring and high precision of the V06 IMERG-F precipitation product will have a superior influence on SPEIs than other commonly used SPPs (Tang et al., 2020; Yu et al., 2020; Peng et al., 2020b).

For the near real-time IMERG-E and IMERG-L precipitation products, the user can acquire the IMERG-E and IMERG-L precipitation products online 4 hr and 14 hr after observation time, respectively (Huffman, et al., 2019). They have attractive timeliness, which can provide useful information for real-time drought monitor and forecast. However, there have been few studies focus on drought monitoring using near real-time SPPs (Sahoo et al., 2015; Lu et al., 2018). Lu et al. (2018) pointed that the SPI values calculated from the research-quality TMPA 3B42 and CMORPH BLD are generally more accuracy than those obtained using near real-time TMPA 3B42RT and CMORPH RAW products over mainland China. Generally, the near real-time IMERG-E and IMERG-L precipitation products have relative lower accuracy than post real-time IMERG-F precipitation product, due to lack of corrections from monthly gauge observations (Jiang et al., 2018; Tan et al., 2019). Our study highlighted that the $SPEI_E$ and $SPEI_L$ demonstrate good performance in CJ, SE, and SW, which indicate a certain potential of the latest near real-time IMERG-E and IMERG-L precipitation product for real-time drought monitor and forecast. However, the $SPEI_E$ and $SPEI_L$ show relative poor performance in NE, NC, NW, XJ and TP, where there are complex terrain, dry climate and few meteorological stations. Therefore, caution should be taken when using the IMERG-E and IMERG-L for real-time monitoring of the drought conditions in some regions of mainland China.

Because of the complex effect of evapotranspiration on drought (Vicente-Serrano et al., 2020), the CC index of GLEAM PET against the reference PET in Fig. 3 is very different from that of SPEIs against SPEIm in Fig. 7, but the RMSE distribution is relatively consistent. This is related to the systematic error between GLEAM PET and reference PET. There are two reasons for the error: a) the calculation methods are different, i.e., the former uses the Priestley–Taylor formula but the latter applies the Penman–Monteith equation; and b) the input data of models are different, i.e., the former adopts gauge-based, reanalysis and satellite-based datasets, whereas the latter only utilizes observation data from meteorological stations. The error of GLEAM PET has a great impact on the accuracy of SPEIs from the RMSE value in Fig. 3 and Fig. 7, especially in the western region, which affects the calculation of SPEIs to some extent.

In addition, the length of the satellite precipitation and PET data will affect the calculation accuracy of SPEI. In this study, we adopted 17 years of IMERG precipitation and GLEAM PET data for calculating SPEI. Although, some previous studies have pointed out those short-term SPPs data can also be used for drought monitoring (Sahoo et al. 2015; Lu et al. 2018). For insurance, Sahoo et al. (2015) suggested that the length of base time period presents very little impact on the conclusions. With the extension of the IMERG retrospective process, longer IMERG precipitation products sequences can be acquired for practical applications, which can effectively solved the problem of data length to some extent (Tang et al., 2020). Overall, our study demonstrates that integration of the latest IMERG precipitation (especially for IMERG-F precipitation) and GLEAM PET products resulted in accurate drought monitoring in China, especially in eastern China and Southwest China.

5.2 General recommendations for future remote-sensing drought monitoring

Different from previous studies, which used satellite precipitation or remote-sensing evapotranspiration to carry out drought research, this study was a preliminary and successful attempt to integrate satellite precipitation and remote-sensing evapotranspiration products for drought monitoring. However, it should be noted that this study only combined limited remote-sensing products, i.e., the IMERG precipitation and GLEAM PET products. Following recent technological advancements, there are many different high-resolution satellite products covering almost every phase of drought propagation (AghaKouchak et al., 2016; Zhang et al., 2019; West et al., 2019).

Remote-sensing drought monitoring should be focused on multiple variables and indicators to provide an integrated measure of drought (Du et al., 2013; Sánchez et al., 2018; Alizadeh and Nikoo, 2018). For instance, Du et al. (2013) proposed an integrated drought index via combining vegetation, temperature and precipitation condition indices by using remotely sensed datasets from MODIS and TRMM. Alizadeh and Nikoo (2018) applied a fusion approach using satellite and reanalysis-based precipitation products, i.e., MERAA-2, GLADS-2, CMAP, GPCP, TRMM, CHOMPS and PERSIANN-CDR, which provided accurate drought analysis. In addition, the combined use of multiple remote-sensing products based drought indices has been able to investigate drought propagation process and response characteristics (Nicolai-Shaw et al., 2017; Orth and Destouni, 2018; Satgé et al., 2019). For example, Nicolai-Shaw et al. (2017) used GLEAM evapotranspiration data as an additional factor for agricultural drought monitoring (by using satellite-derived soil moisture observations) to explore the link between evapotranspiration and vegetation. Satgé et al. (2019) unravelled the impacts of droughts on water resources by integrated use of CHIRPS precipitation, GLEAM potential evapotranspiration, GRACE total water storage and AVHRR vegetation condition datasets.

6 Conclusion

This study primarily evaluated the precision characteristics of the latest long-term V06 IMERG precipitation (i.e., IMERG-E, IMERG-L and IMERG-F) and GLEAM PET products and assessed their drought monitoring utility over mainland China. The observed precipitation and calculated PET of meteorological stations from China Meteorological Administration were adopted as reference data to evaluate IMERG precipitation and GLEAM PET. SPEI, a widely used meteorological drought index, was selected to verify the potential utility of IMERG precipitation and GLEAM PET products in drought monitoring. The major conclusions are as follows:

(1) The IMERG-F presented much better performance than IMERG-E and IMERG-L in terms of higher CC values and smaller BIAS and RMSE values. There was high consistency (with average CC of 0.92), small deviation (with average BIAS of 10%) and low error (with average RMSE of 26.42 mm/month) between IMERG-F precipitation and gauge observation over mainland China. Overall, IMERG precipitation products, especially for the IMERG-F product, fitted with the gauge observation well in most areas, except for XJ and TP. GLEAM PET could well simulate the trend of the reference PET in China, whereas it had larger deviation and error in NW, XJ and TP, and it underestimated the reference PET data there.

(2) In general, the $SPEI_F$ demonstrated much better performance than $SPEI_E$ and $SPEI_L$ over mainland China. From the grid and regional comprehensive evaluation, the $SPEI_F$ had good performance in eastern China and SW, in terms of high CC, small RMSE and good POD and FAR. The $SPEI_E$ and $SPEI_L$ demonstrated good performance in CJ, SE, and SW. Due to lack of corrections from gauge observations, caution should be taken when using the IMERG-E and IMERG-L for real-time monitoring of the drought conditions in some specific regions of mainland China.

(3) For typical drought event evaluation, SPEIs had some small deviations in terms of drought intensity and drought area in local areas. Generally, they could well capture the evolution of drought events and the spatial characteristics of a typical drought event in a specific month, indicating that the IMERG precipitation (especially for IMERG-F) and

GLEAM PET are useful in detecting the timing, intensity and magnitude of drought events.

In conclusion, SPEIs based on IMERG precipitation (especially for IMERG-F) and GLEAM PET products are suitable for drought monitoring in eastern China and SW, which shows that it has a good potential to monitor drought by integrating satellite precipitation and PET products under the principle of water balance. Remote-sensing products can be used as attractive data inputs for drought monitoring and analysis. However, in this study, we only combined a limited number of remote-sensing products. In the future, we should further strengthen the drought propagation process and the response characteristics research by integrating multiple high-resolution remote-sensing products.

ACKNOWLEDGMENTS

The National Key Research and Development Program approved by Ministry of Science and Technology, China (2016YFA0601504); National Natural Science Foundation of China (51979069 and 41807165); Fundamental Research Funds for the Central Universities (B200204029); National Natural Science Foundation of Jiangsu Province, China (BK20180512).

REFERENCES

Alizadeh, M., Nikoo, M., 2018. A fusion-based methodology for meteorological drought estimation using remote sensing data. Remote Sens. Environ. 211, 229–247

AghaKouchak, A., Farahmand, A., Melton, F.S., Teixeira, J., Anderson, M.C., Wardlow, B.D., Hain, C.R., 2015. Remote sensing of drought: Progress, challenges and opportunities. Rev. Geophys. 53 (2), 452–480.

Agutu, N., Awange, J., Zerihun, A., Ndehedehe, C., Kuhn, M., Fukuda, Y., 2017. Assessing multi-satellite remote sensing, reanalysis, and land surface models' products in characterizing agricultural drought in East Africa. Remote Sens. Environ. 194, 287-302.

Allen, R., Pereira, L., Raes, D., Smith, M., 1998. Crop Evapotranspiration: Guidelines for Computing Crop Water Requirements. United Nations Food and Agriculture Organization, Irrigation and Drainage Paper, 56.

Bai, X., Shen, W., Wu, X., Wang, P., 2020. Applicability of long-term satellite-based precipitation products for drought indices considering global warming. J. Environ. Manag. 255, 109846.

Beguerıa, S., Vicente-Serrano, S., Reig, F., Latorre, B., 2014. Standardized precipitation evapotranspiration index (SPEI) revisited: parameter fitting, evapotranspiration models, tools, datasets and drought monitoring. Int. J. Climatol. 34, 3001–3023

Bayissa, Y., Tadesse, T., Demisse, G., Shiferaw, A., 2017. Evaluation of satellite-based rainfall estimates and application to monitor meteorological drought for the Upper Blue Nile Basin, Ethiopia. Remote Sens. 9(7), 669.

Chawla, I., Karthikeyan, L., Mishra, A.K., 2020. A review of remote sensing applications for water security: Quantity, quality, and extremes. J. Hydrol. 585, 124826.

Chen, S., Hong, Y., Cao, Q., Gourley, J.J., Kirstetter, P., Yong, B., 2013. Similarity and difference of the two successive v6 and v7 trmm multisatellite precipitation analysis performance over china. J. Geophys. Res. Atmos., 118, 13060-13074.

Chen, C., Chen, Q., Duan, Z., Zhang, J., Mo, K., Li, Z., Tang, G., 2018. Multiscale Comparative Evaluation of the GPM IMERG v5 and TRMM 3B42 v7 Precipitation Products from 2015 to 2017 over a Climate Transition Area of China. Remote Sens. 10, 944.

Chen, S., Zhang, L., Zhang, Y., Guo, M., Liu, X., 2020. Evaluation of Tropical Rainfall Measuring Mission (TRMM) satellite precipitation products for drought monitoring over the middle and lower reaches of the Yangtze River Basin, China. J. Geogr. Sci. 30(1): 53-67.

Dai, A., 2011. Characteristics and trends in various forms of the Palmer Drought Severity Index during 1900–2008. J. Geophys. Res. Atmos. 116(D12).

Duan, Z., Tuo, Y., Liu, J., Gao, H., Song, X., Zhang, Z., Yang, L., Mekonnen, D., 2019. Hydrological evaluation of open-access precipitation and air temperature datasets using SWAT in a poorly gauged basin in Ethiopia. J. Hydrol. 556, 612-626.

Du, L., Tian, Q., Yu, T., Meng, Q., Jancso, T., Udvardy, P., Huang, Y., 2013. A comprehensive drought monitoring method integrating MODIS and TRMM data. Int. J. Appl. Earth Obs. Geoinf. 23, 245–253.

Funk, C., Peterson, P., Landsfeld, M., Pedreros, D., Verdin, J., Shukla, S., Husak, G., Rowland, J., Harrison, L., Hoell, A., Michaelsen, J., 2015. The climate hazards infrared precipitation with stations—a new environmental record for monitoring extremes. Sci. Data. 2, 150066.

Gao, Z., Long, D., Tang, G., Zeng, C., Huang, J., Hong, Y., 2017. Assessing the potential of satellite-based precipitation estimates for flood frequency analysis in ungauged or poorly gauged tributaries of China's Yangtze River basin. J. Hydrol. 550, 478-496.

Guo, H., Chen, S., Bao, A., Behrangi, A., Hong, Y., Ndayisaba, F., Hu, J., Stepanian, P.M., 2016. Early assessment of integrated multi-satellite retrievals for global precipitation measurement over China. Atmos. Res. 176, 121-133.

Hou, A., Kakar, R., Neeck, S., Azarbarzin, A., Kummerow, C., Kojima, M., Oki, R., Nakamura, K., Iguchi, T., 2014. The global precipitation measurement mission. Bull. Am. Meteorol. Soc. 95(5), 701-722.

Huffman, G., Bolvin, D., Nelkin, E., Wolff, D., Adler, R., Gu, G., Hong, Y., Bowman K., Stocker, E., 2007. The TRMM multisatellite precipitation analysis (TMPA): Quasi-global, multiyear, combined-sensor precipitation estimates at fine scales. J. Hydrometeorol. 8 (1), 38–55.

Huffman, G.J., Bolvin, D.T., Braithwaite, D., Hsu, K., Joyce, R., Xie, P., Yoo, S.H., 2015. NASA global precipitation measurement (GPM) integrated multi-satellite retrievals for GPM (IMERG). Algorithm theoretical basis document, 4, 30.

Huffman, G.J., Bolvin, D.T., Braithwaite, D., Hsu, K., Joyce, R., Kidd, C., Nelkin, E.J., Sorooshian, S., Tan, J., Xie, P., 2019. NASA Global Precipitation Measurement (GPM) Integrated Multi-satellitE Retrievals for GPM (IMERG). In: Algorithm Theoretical Basis Document (ATBD) Version 06. NASA/GSFC, Greenbelt, MD, USA.

Jiang, S., Ren, L., Hong, Y., Yong, B., Yang, X., Yuan, F., Ma, M., 2012. Comprehensive evaluation of multi-satellite precipitation products with a dense rain gauge network and optimally merging their simulated hydrological flows using the Bayesian model averaging method. J. Hydrol. 452-453, 213-225.

Jiang, S., Ren, L., Zhou, M., Yong, B., Zhang, Y., Ma, M., 2017. Drought monitoring and reliability evaluation of the latest TMPA precipitation data in the Weihe River Basin, Northwest China. J. Arid Land. 9(2), 256–269.

Jiang, S., Ren, L., Xu, C-Y., Yong, B., Yuan, F., Liu, Y., Yang, X., Zeng, X., 2018. Statistical and hydrological evaluation of the latest Integrated Multi-satellitE Retrievals for GPM (IMERG) over a midlatitude humid basin in South China. Atmos. Res. 214, 418–429.

Jiang, S., Wang, M., Ren, L., Xu, C-Y., Yuan, F., Liu, Y., Lu, Y, Shen, H, 2019. A framework for quantifying the impacts of climate change and human activities on hydrological drought in a semiarid basin of Northern China. Hydrol. Process. 33(7), 1075-1088.

Jiang, S., Liu, R., Ren, L., Wang, M., Shi, J., Zhong, F., Duan, Z., 2020: Evaluation and hydrological application of CMADS against TMPA 3B42V7, CMORPH-BLD, CHIRPS, and PERSIANN-CDR in the Upper Huaihe River Basin, China. J. Meteor. Res., doi: 10.1007/s13351-020-0026-6.

Joyce, R., Janowiak, J., Arkin, P., Xie, P., 2004. CMORPH: A method that produces global precipitation estimates from passive microwave and infrared data at high spatial and temporal resolution. J. Hydrometeorol. 5 (3), 487–503.

Li, J., Wang, Z. L., Wu, X. S., Xu, C-Y., Guo, S. L., Chen, X. H. 2020. Toward Monitoring Short-Term Droughts Using a Novel Daily-Scale, Standardized Antecedent Precipitation Evapotranspiration Index. J. Hydrometeorol. 21, 891-908.

Lloyd-Hughes, B., 2014. The impracticality of a universal drought definition. Theor. Appl. Climatol. 117(3-4), 607-611.

Lu, J., Jia, L., Menenti, M., Yan, Y., Zheng, C., Zhou, J., 2018. Performance of the Standardized Precipitation Index based on the TMPA and CMORPH precipitation products for drought monitoring in China. IEEE J. Sel. Top. Appl. Earth Observ. Remote Sens. 11 (5), 1387–1396.

Lu, Y., Jiang, S., Ren, L., Zhang, L., Wang, M., Liu, R., Wei, L., 2019. Spatial and Temporal Variability in Precipitation Concentration over Mainland China, 1961–2017. Water, 11(5), 881.

McKee, T.B., Doesken, N.J., Kleist, J., 1993. The relationship of drought frequency and duration to time scales. In Proceedings of the 8th Conference on Applied Climatology. American Meteorological Society, Boston, MA.

Miralles, D., Holmes, T., De Jeu, R., Gash, J., Meesters, A., Dolman, A., 2011. Global land-surface evaporation estimated from satellite-based observations. Hydrol. Earth Syst. Sci. 15(2):453-469.

Martens, B., Miralles, D., Lievens, H., Schalie, R., De Jeu, R., Fernández-Prieto, D., Beck, H., Dorigo, W., Verhoest, N., 2017. GLEAM v3: satellite-based land evaporation and root-zone soil moisture. Geosci. Model Dev. 10, 1903–1925.

Martens, B., De Jeu, R., Verhoest, N., Schuurmans, H., Kleijer, J., Miralles, D., 2018. Towards Estimating Land Evaporation at Field Scales Using GLEAM. Remote Sens., 10(11), 1720.

Mishra, A.K., Singh, V.P., 2010. A review of drought concepts. J. Hydrol. 391(1-2), 202-216.

Moran, M., Clarke, T., Inoue, Y., Vidal, A. 1994. Estimating crop water deficit using the relation between surface-air temperature and spectral vegetation index. Remote Sens. Environ., 49(3), 246–263.

Mu, Q., Heinsch, F., Zhao, M., Running, S., 2007. Development of a global evapotranspiration algorithm based on MODIS and global meteorology data. Remote Sens. Environ. 111(4), 519-536.

Mu, Q., Zhao, M., Running, S., 2011. Improvements to a MODIS global terrestrial evapotranspiration algorithm. Remote Sens. Environ. 115(8), 1781-1800.

Nicolai-Shaw, N., Zscheischler, J., Hirschi, M., Gudmundsson, L., Seneviratne, S., 2017. A drought event composite analysis using satellite remote-sensing based soil moisture. Remote Sens. Environ. 203, 216-225.

Orth, R., Destouni, G. 2018. Drought reduces blue-water fluxes more strongly than green-water fluxes in Europe. Nat. Commun. 9, 3602.

Palmer, W.C., 1965. Meteorological Drought. US Department of Commerce, Weather Bureau, Washington, DC.

Peng, J., Dadson, S., Hirpa, F., Dyer, E., Lees, T., Miralles, D. G., Vicente-Serrano, S. M., Funk, C., 2020a. A pan-African high-resolution drought index dataset. Earth Syst. Sci. Data, 12, 753–769.

Peng, F., Zhao, S., Chen, C., Cong, D., Wang, Y., Ouyang, H., 2020b. Evaluation and comparison of the precipitation detection ability of multiple satellite products in a typical agriculture area of China. Atmos. Res. 236, 104814.

Sahoo, A.K., Sheffield, J., Pan, M., Wood, E.F., 2015. Evaluation of the tropical rainfall measuring mission multi-satellite precipitation analysis (TMPA) for assessment of large-scale meteorological drought. Remote Sens. Environ. 159, 181-193.

Sandholt, I., Rasmussen, K., Andersen, J., 2002. A simple interpretation of the surface temperature/vegetation index space for assessment of surface moisture status. Remote Sens. Environ. 79(2-3), 213-224.

Sánchez, N., González-Zamora, A., Martínez-Fernández, J., Piles, M., Pablos, M., 2018. Integrated remote sensing approach to global agricultural drought monitoring. Agric. For. Meteorol. 259, 141–153.

Satgé, F., Hussain, Y., Xavier, A., Zolá, R. P., Salles, L., Timouk, F., Seyler, F., Garnier, J., Frappart, F., Bonnet, M.P., 2019. Unraveling the impacts of droughts and agricultural intensification on the Altiplano water resources. Agric. For. Meteorol. 279, 107710.

Sheffield, J., Wood, E.F., Roderick, M.L., 2012. Little change in global drought over the past 60 years. Nature, 491, 435-438.

Shen, Y., Xiong, A., Wang, Y., Xie, P., 2010. Performance of high-resolution satellite precipitation products over China. J. Geophys. Res. Atmos. 115(D2).

Shukla, S., Wood, A.W., 2008. Use of a standardized runoff index for characterizing hydrologic drought.

Geophys. Res. Lett. 35(2), L02405.

Sorooshian, S., Hsu, K., Gao, X., Gupta, H., Imam, B., Braithwaite, D., 2000. Evaluation of PERSIANN system satellite-based estimates of tropical rainfall. Bull. Am. Meteorol. Soc. 81(9), 2035-2046.

Tan, J., Huffman, G., Bolvin, D., Nelkin, E., 2019. Diurnal Cycle of IMERG V06 Precipitation. Geophys. Res. Lett. 46.

Trenberth, K., Dai, A., Schrier, G., Jones, P., Barichivich, J., Briffa, K., Sheffield, J., 2014. Global warming and changes in drought. Nat. Clim. Chang. 4, 17–22.

Tang, G., Clark, M., Papalexiou, S, Ma, Z., Hong, Y., 2020. Have satellite precipitation products improved over last two decades? A comprehensive comparison of GPM IMERG with nine satellite and reanalysis datasets. Remote Sens. Environ. 240, 111697.

Vicente-Serrano, S.M., Beguería, S., López-Moreno, J.I., 2010. A multiscalar drought index sensitive to global warming: the standardized precipitation evapotranspiration index. J. Clim. 23, 1696–1718.

Vicente-Serrano, S.M., Beguería, S., López-Moreno, J.I., 2011. Comment on "Characteristics and trends in various forms of the Palmer Drought Severity Index (PDSI) during 1900–2008" by Aiguo Dai. J. Geophys. Res.: Atmos. 116, D19112.

Vicente-Serrano, S., Miralles, D., Domínguez-Castro, F., Azorin-Molina, C., El Kenawy, A., McVicar, T., Tomas-Burguera, M., Beguería, S., Maneta, M., Peña-Gallardo, M., 2018. Global assessment of the Standardized Evapotranspiration Deficit Index (SEDI) for drought analysis and monitoring. J. Clim. 31(14), 5371-5393.

Vicente-Serrano, S., McVicar, T., Miralles, D., Yang, Y., Tomas-Burguera, M. 2020. Unraveling the influence of atmospheric evaporative demand on drought and its response to climate change. WIREs Clim Change. 11(2), e632.

Wang, C., Tang, G., Han, Z., Guo, X., Hong, Y., 2018. Global intercomparison and regional evaluation of GPM IMERG Version-03, Version-04 and its latest Version-05 precipitation products: Similarity, difference and improvements. J. Hydrol. 564, 342-356.

Wang, Z., Li, J., Lai, C., Zeng, Z., Zhong, R., Chen, X., Zhou, X., Wang, M., 2017a. Does drought in China show a significant decreasing trend from 1961 to 2009?. Sci. Total Environ. 579, 314–324.

Wang, Z., Zhong, R., Lai, C., 2017b. Evaluation and hydrologic validation of TMPA satellite precipitation product downstream of the Pearl River Basin, China. Hydrol. Process. 31(23), 4169-4182.

Wei, L., Jiang, S., Ren, L., Yuan, F., Zhang, L., 2019. Performance of Two Long-Term Satellite-Based and GPCC 8.0 Precipitation Products for Drought Monitoring over the Yellow River Basin in China. Sustainability, 11(18), 4969.

West, H., Quinn, N., Horswell, M., 2019. Remote sensing for drought monitoring & impact assessment: Progress, past challenges and future opportunities. Remote Sens. Environ. 232, 111291.

Xu, Z., Wu, Z., He, H., Wu, X., Zhou, J., Zhang, Y., Guo, X., 2019. Evaluating the accuracy of MSWEP V2. 1 and its performance for drought monitoring over mainland China. Atmos. Res. 226, 17-31.

Yuan, F., Wang, B., Shi, C., Cui, W., Zhao, C., Liu, Y., Ren, L., Zhang, L., Zhu, Y., Chen, T., Jiang, S., 2018. Evaluation of hydrological utility of IMERG Final run V05 and TMPA 3B42V7 satellite precipitation products in the Yellow River source region, China. J. Hydrol. 567, 696-711.

Yu, C., Hu, D.Y., Liu, M.Q., Wang, S.S., Di, Y.F.., 2020. Spatio-temporal accuracy evaluation of three high-resolution satellite precipitation products in China area. Atmos. Res. 241, 104952.

Yu, M., Li, Q., Hayes, M., Svoboda, M., Heim, R. 2014. Are droughts becoming more frequent or severe in China based on the standardized precipitation evapotranspiration index: 1951–2010?. Int. J. Climatol. 34(3), 545-558.

Zambrano, F., Wardlow, B., Tadesse, T., Lillo-Saavedra, M., Lagos, O., 2017. Evaluating satellite-derived long-term historical precipitation datasets for drought monitoring in Chile. Atmos. Res. 186, 26-42.

Zhang, L., Liu, Y., Ren, L., Jiang, S., Yang, X., Yuan, F., Wang, M., Wei, L., 2019. Drought Monitoring and Evaluation by ESA CCI Soil Moisture Products Over the Yellow River Basin. IEEE J. Sel. Top. Appl. Earth Observ. Remote Sens. 12(9), 3376-3386.

Zhang, W., Jin, F., Zhao, J., Qi, L., Ren, H., 2013. The possible influence of a nonconventional El Niño on the severe autumn drought of 2009 in Southwest China. J. Clim. 26(21), 8392-8405.

Zhang, Y. Q., Kong, D. D., Gan, R., Chiew, F. H. S., McVicar, T. R., Zhang, Q., Yang, Y. T., 2019. Coupled estimation of 500m and 8-day resolution global evapotranspiration and gross primary production in 2002–2017. Remote Sens. Environ. 222, 165-182.

Zhao, H.G., Ma, Y.F., 2019. Evaluating the Drought-Monitoring Utility of Four Satellite-Based Quantitative Precipitation Estimation Products at Global Scale. Remote Sens. 11(17), 2010.

Zhong, R.D., Chen, X.H., Lai, C.G., Wang, Z.L., Lian, Y.Q., Yu, H.J., Wu, X.Q., 2019. Drought monitoring utility of satellite-based precipitation products across mainland China. J. Hydrol. 568, 343-359.

Table 1. Drought classification based on Standardized Precipitation Evapotranspiration Index (SPEI) values.

Drought class	SPEI values
No drought	SPEI > -0.5
Light drought	-1.0 < SPEI ≤ -0.5
Moderate drought	-1.5 < SPEI ≤ -1.0
Severe drought	-2.0 < SPEI ≤ -1.5
Extreme drought	SPEI ≤ -2.0

Table 2. 5%, 50% and 95% quantiles of the CC, BIAS, RMSE for monthly IMERG-E, IMERG-L and IMERG-F precipitation, and GLEAM PET in eight regions.

Region	Quantile	IMERG-E			IMERG-L			IMERG-F			GLEAM		
		CC	BIAS (%)	RMSE (mm/month)	CC	BIAS (%)	RMSE (mm/month)	CC	BIAS (%)	RMSE (mm/month)	CC	BIAS (%)	RMSE (mm/month)
NE	5%	0.66	-8	25.29	0.65	-7	24.80	0.90	2	11.43	0.92	-46	9.17
	50%	0.80	21	40.71	0.81	24	41.67	0.96	12	18.38	0.96	-25	20.52
	95%	0.86	58	65.84	0.87	65	71.00	0.98	28	29.76	0.99	-11	40.23
NC	5%	0.77	-1	31.75	0.77	0	31.61	0.91	-6	14.34	0.91	-33	10.78
	50%	0.84	20	41.93	0.84	21	43.63	0.95	8	21.82	0.96	-20	20.43
	95%	0.89	51	67.62	0.89	56	73.04	0.97	22	39.01	0.98	-7	31.12
CJ	5%	0.73	-11	40.96	0.73	-12	39.67	0.89	-6	22.16	0.96	-18	6.52
	50%	0.82	12	62.28	0.82	12	61.88	0.94	6	33.23	0.98	-9	9.96
	95%	0.86	33	80.99	0.87	34	82.97	0.97	17	47.58	0.99	1	18.21
SE	5%	0.72	-20	56.21	0.75	-22	57.83	0.89	-11	27.67	0.81	-18	6.01
	50%	0.84	0	72.78	0.85	-2	71.99	0.95	4	41.96	0.97	-7	11.27
	95%	0.91	17	110.37	0.90	15	108.69	0.98	19	71.79	0.99	11	23.86
SW	5%	0.73	-40	35.95	0.74	-44	33.92	0.90	-19	20.83	0.77	-29	6.72
	50%	0.85	-9	50.37	0.85	-9	50.08	0.95	3	29.95	0.97	-9	10.94
	95%	0.92	10	87.22	0.92	8	85.68	0.98	24	51.91	0.99	3	32.24
NW	5%	0.67	-16	13.23	0.71	-17	12.26	0.85	-8	6.57	0.93	-70	10.76
	50%	0.82	16	24.68	0.82	19	24.61	0.96	6	11.69	0.96	-41	34.46
	95%	0.88	91	39.03	0.89	108	43.37	0.98	49	19.52	0.98	-14	78.68
XJ	5%	0.36	-47	6.81	0.40	-53	6.40	0.60	-41	3.95	0.94	-71	20.22
	50%	0.59	42	16.97	0.62	35	16.28	0.79	16	10.50	0.98	-56	52.96
	95%	0.80	265	33.36	0.81	277	35.44	0.93	132	23.46	0.99	-30	87.01
TP	5%	0.65	-51	8.26	0.68	-53	7.71	0.80	-20	6.30	0.76	-64	18.33
	50%	0.84	-33	28.30	0.85	-34	27.80	0.96	2	14.40	0.90	-32	26.86
	95%	0.92	51	42.23	0.93	43	42.59	0.98	139	31.59	0.97	-10	54.35

Table 3. 5%, 50%, and 95% quantiles of CC, RMSE, POD and FAR for the SPEIs ($SPEI_E$, $SPEI_L$, $SPEI_F$) at 3-month timescale in eight regions.

Region	Quantile	$SPEI_E$				$SPEI_L$				$SPEI_F$			
		CC	RMSE	POD	FAR	CC	RMSE	POD	FAR	CC	RMSE	POD	FAR
NE	5%	0.49	0.72	0.47	0.28	0.49	0.70	0.52	0.26	0.67	0.43	0.64	0.14
	50%	0.60	0.90	0.60	0.39	0.62	0.89	0.61	0.39	0.82	0.61	0.76	0.25
	95%	0.74	1.09	0.70	0.50	0.75	1.08	0.73	0.50	0.91	0.89	0.85	0.38
NC	5%	0.46	0.70	0.48	0.29	0.49	0.69	0.51	0.27	0.66	0.35	0.63	0.15
	50%	0.61	0.90	0.61	0.39	0.62	0.90	0.62	0.38	0.82	0.63	0.76	0.25
	95%	0.76	1.11	0.72	0.48	0.77	1.09	0.74	0.47	0.94	0.92	0.87	0.35
CJ	5%	0.57	0.65	0.55	0.24	0.58	0.64	0.55	0.23	0.76	0.33	0.69	0.10
	50%	0.71	0.78	0.66	0.34	0.72	0.76	0.67	0.33	0.88	0.49	0.81	0.18
	95%	0.79	0.99	0.76	0.44	0.80	0.99	0.77	0.44	0.95	0.76	0.90	0.29
SE	5%	0.55	0.59	0.57	0.22	0.59	0.56	0.56	0.21	0.74	0.32	0.68	0.11
	50%	0.73	0.76	0.69	0.32	0.73	0.73	0.69	0.31	0.89	0.48	0.79	0.20
	95%	0.83	0.96	0.78	0.44	0.84	0.96	0.79	0.44	0.95	0.78	0.89	0.33
SW	5%	0.47	0.74	0.53	0.28	0.47	0.72	0.54	0.26	0.62	0.46	0.67	0.16
	50%	0.60	0.93	0.63	0.38	0.62	0.90	0.66	0.37	0.79	0.68	0.76	0.25
	95%	0.73	1.08	0.74	0.47	0.74	1.13	0.74	0.45	0.90	1.00	0.86	0.34
NW	5%	0.32	0.78	0.46	0.27	0.33	0.76	0.46	0.28	0.50	0.51	0.57	0.17
	50%	0.55	0.97	0.60	0.40	0.57	0.93	0.59	0.40	0.77	0.69	0.71	0.29
	95%	0.70	1.23	0.72	0.54	0.71	1.25	0.71	0.51	0.87	1.07	0.83	0.43
XJ	5%	0.16	0.95	0.32	0.39	0.12	0.93	0.33	0.36	0.19	0.64	0.41	0.26
	50%	0.37	1.13	0.49	0.51	0.41	1.14	0.50	0.49	0.57	0.94	0.58	0.40
	95%	0.56	1.42	0.62	0.68	0.57	1.42	0.63	0.63	0.80	1.32	0.77	0.59
TP	5%	0.27	0.87	0.40	0.28	0.27	0.84	0.41	0.27	0.40	0.69	0.48	0.20
	50%	0.49	1.06	0.58	0.41	0.50	1.07	0.58	0.40	0.64	0.92	0.66	0.32
	95%	0.66	1.31	0.70	0.60	0.67	1.31	0.71	0.60	0.78	1.27	0.77	0.52

Table 4. Information of the four typical drought events in terms of references and Fig. 9 in NE, NC, CJ and SW.

Region	Start–end time	Severity	Intensity	Timescale of drought index	Reference
NE	December 2001 to November 2002	-9.84	-0.89	12	Zhong et al., 2019
NC	December 2010 to June 2011	-7.83	-1.12	3	Xu et al., 2019
CJ	March 2011 to September 2011	-8.38	-1.18	6	Chen et al., 2020
SW	September 2009 to April 2010	-7.9	-0.99	3	Zhang et al., 2013

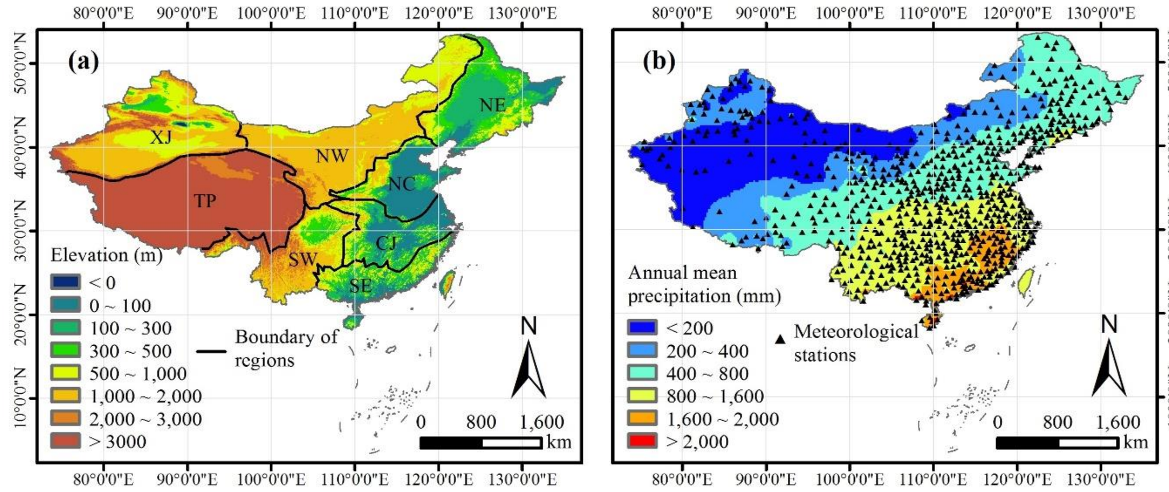

Fig. 1. The digital elevation model (DEM) and spatial distribution of 807 meteorological stations and eight sub-regions over mainland China. Note: NE, Northeast China; NC, Northern China; CJ, the middle and lower reaches of the Yangtze River region; SE, Southeast China; SW, Southwest China; NW, Northwest China; XJ, Xinjiang; TP, Qinghai–Tibet Plateau.

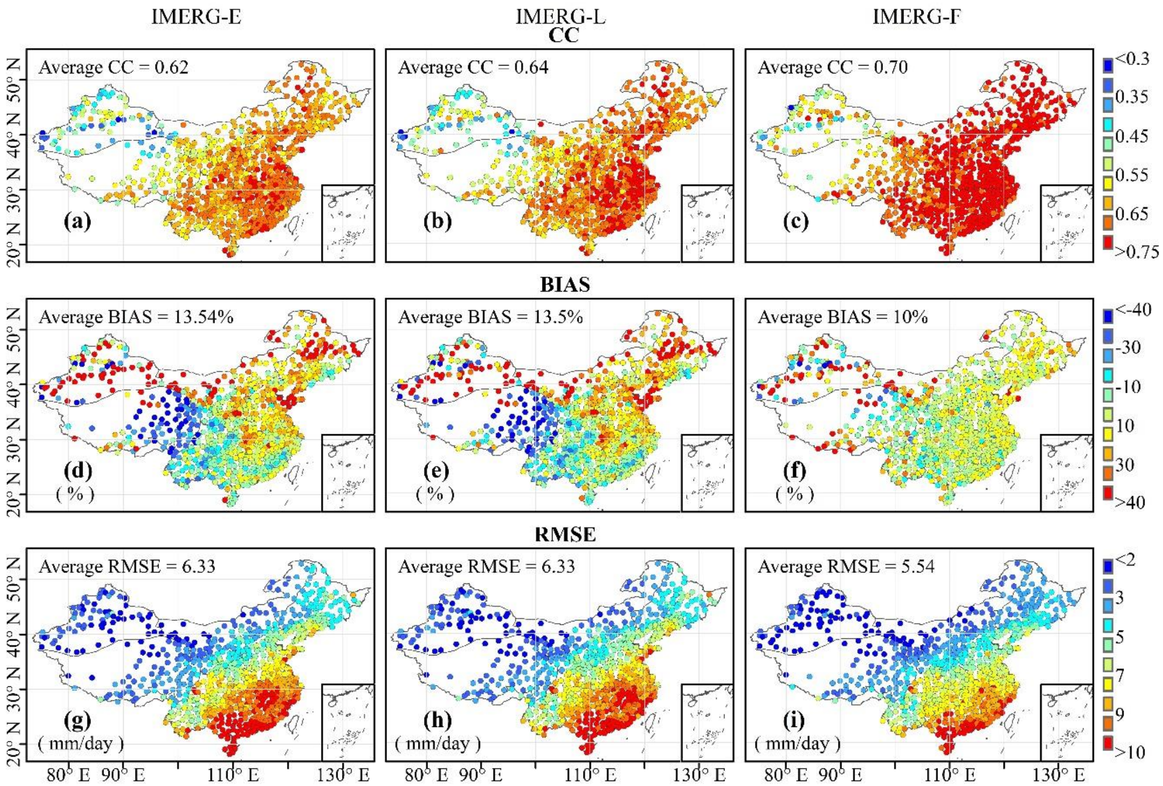

Fig. 2. Spatial distribution of the (a-c) CC, (d-f) BIAS, (g-i) RMSE for IMERG three Runs products (IMERG-E, IMERG-L and IMERG-F) versus precipitation from meteorological stations at daily scale over mainland China.

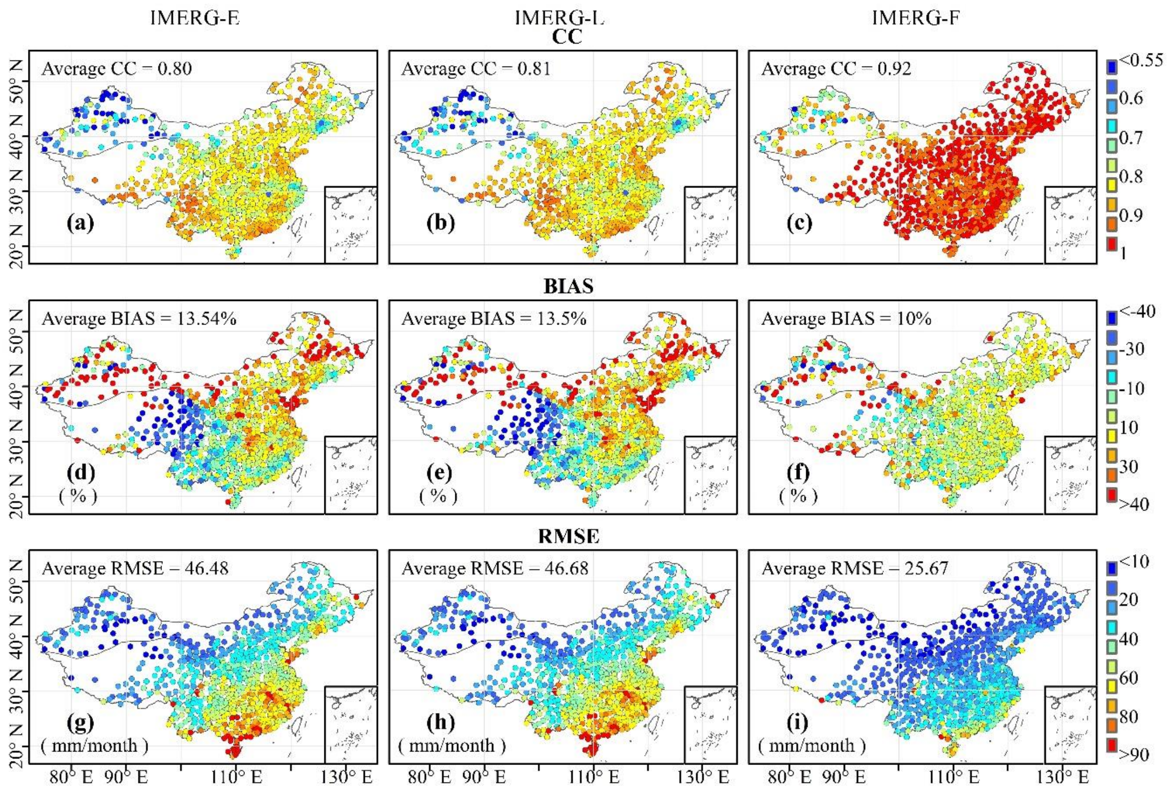

Fig. 3. Spatial distribution of the (a-c) CC, (d-f) BIAS, (g-i) RMSE for IMERG three Runs products (IMERG-E, IMERG-L and IMERG-F) versus precipitation from meteorological stations at monthly scale over mainland China.

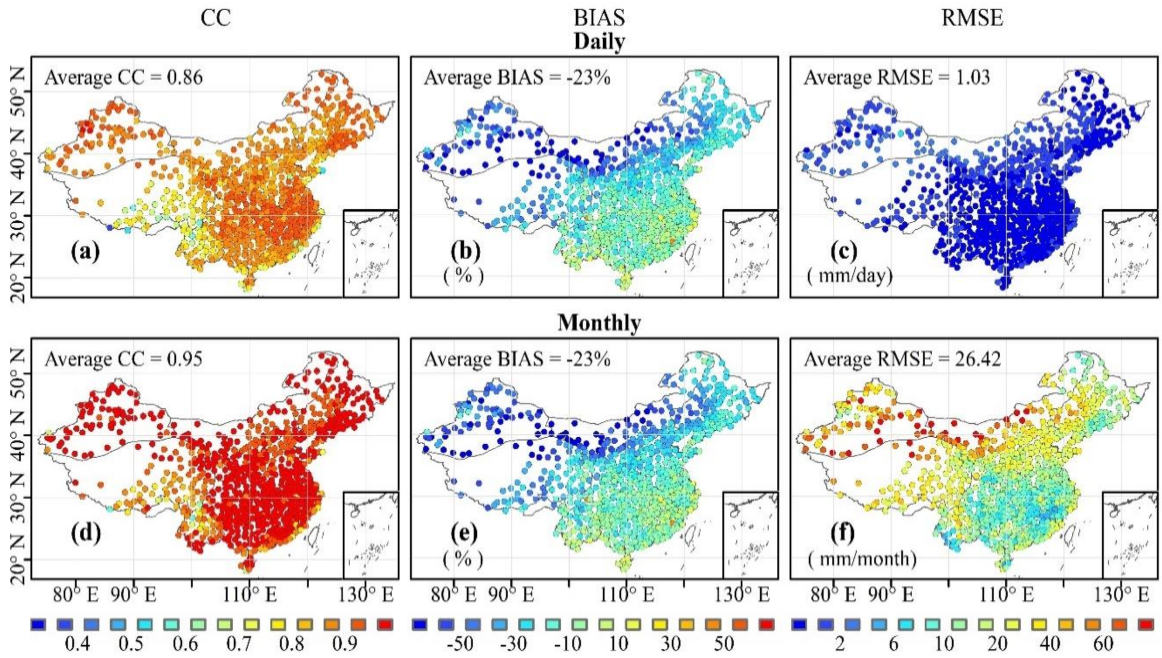

Fig. 4. Spatial distribution of the (a) daily CC, (b) daily BIAS, (c) daily RMSE, (d) monthly CC, (e) monthly BIAS, and (f) monthly RMSE for GLEAM PET versus PET from meteorological stations over mainland China.

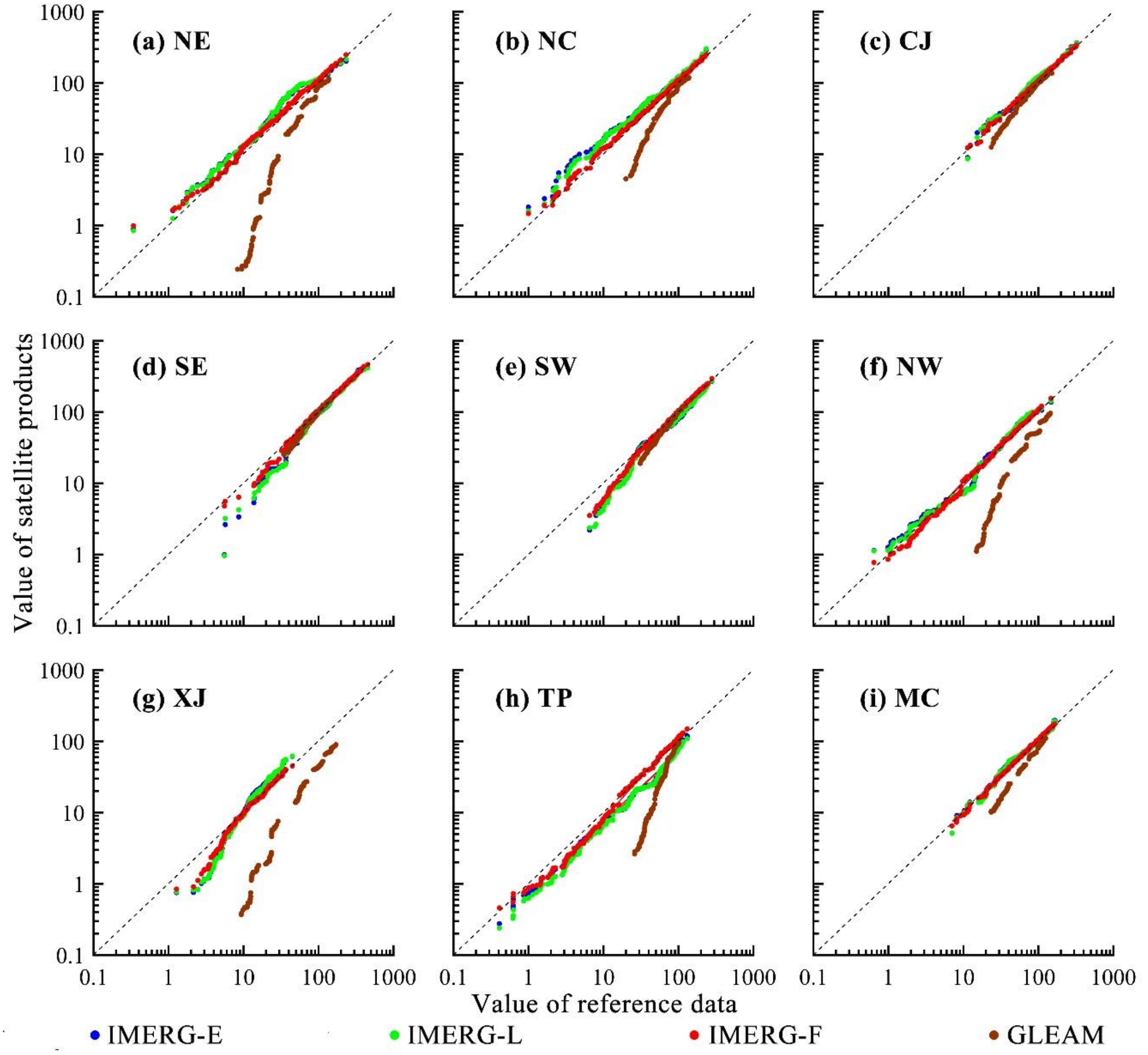

Fig. 5. Q–Q plot of the regionally averaged IMERG-E, IMERG-L, and IMERG-F versus gauge precipitation (mm/month) and GLEAM versus reference PET (mm/month) in eight regions and MC from 2001 to 2017. Note: MC, mainland China.

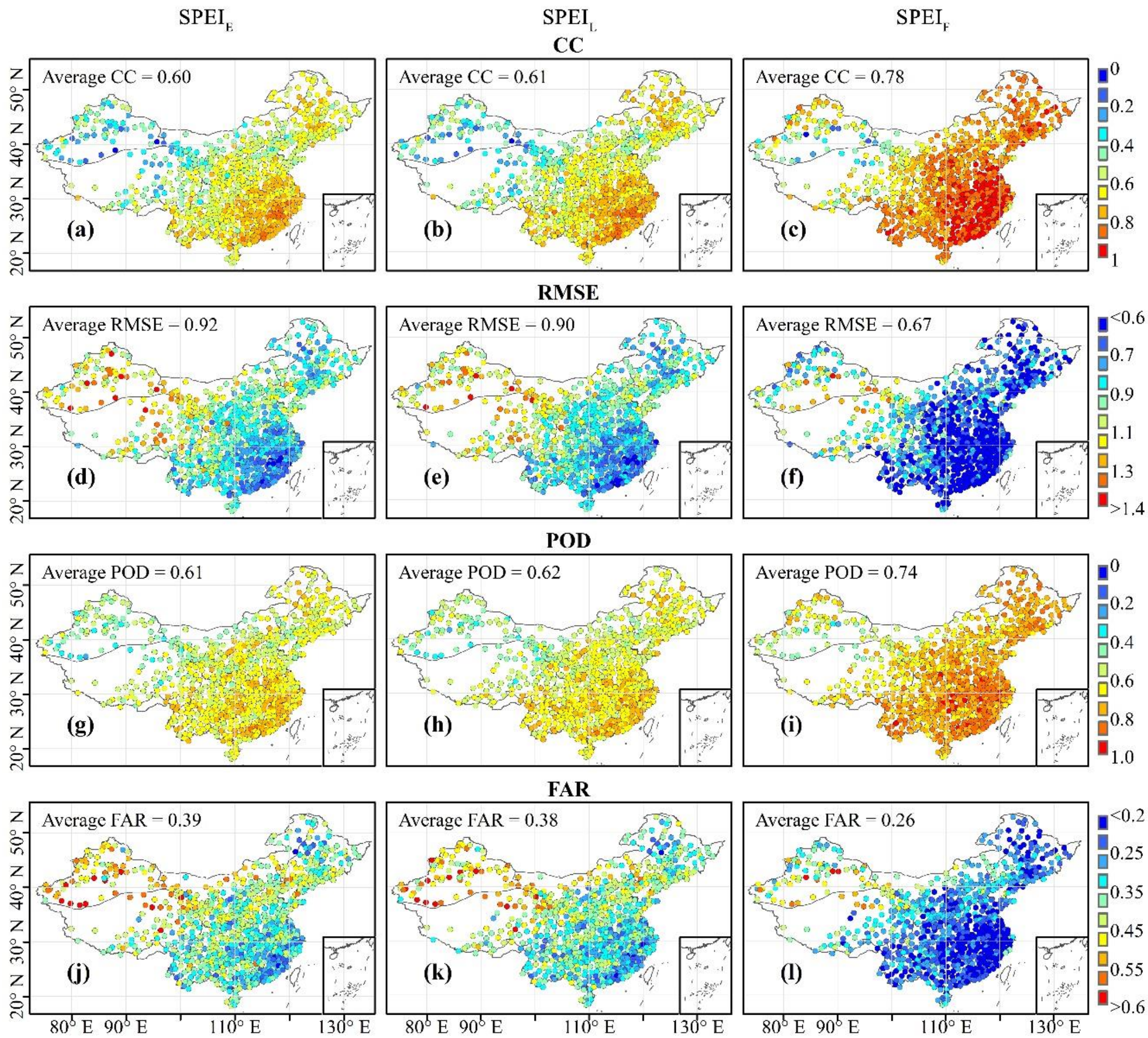

Fig. 6. Spatial distribution of the (a-c) CC, (d-f) RMSE, (g-i) POD and (j-l) FAR for the SPEIs (SPEI$_E$, SPEI$_L$ and SPEI$_F$) against SPEIm at 3-month timescale.

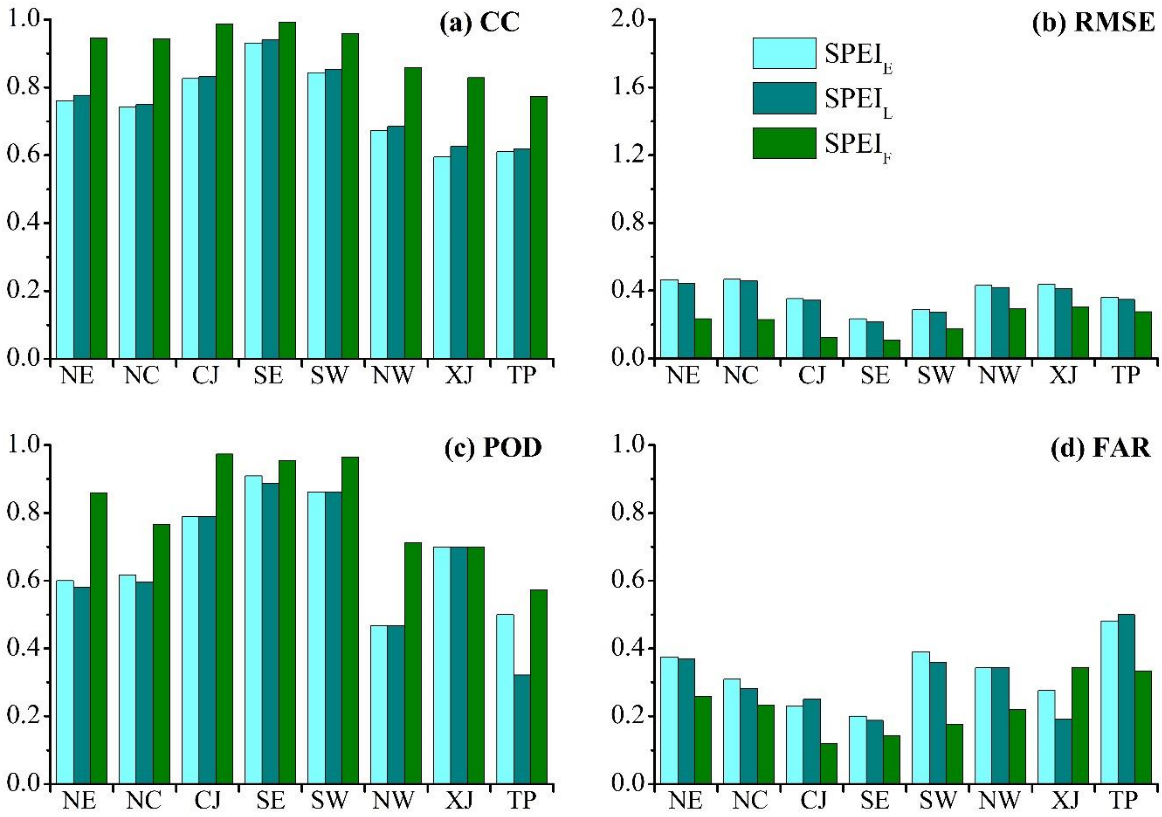

Fig. 7. CC, RMSE, POD and FAR of regional SPEIs (SPEI$_E$, SPEI$_L$ and SPEI$_F$) against SPEIm at 3-month timescale in eight regions.

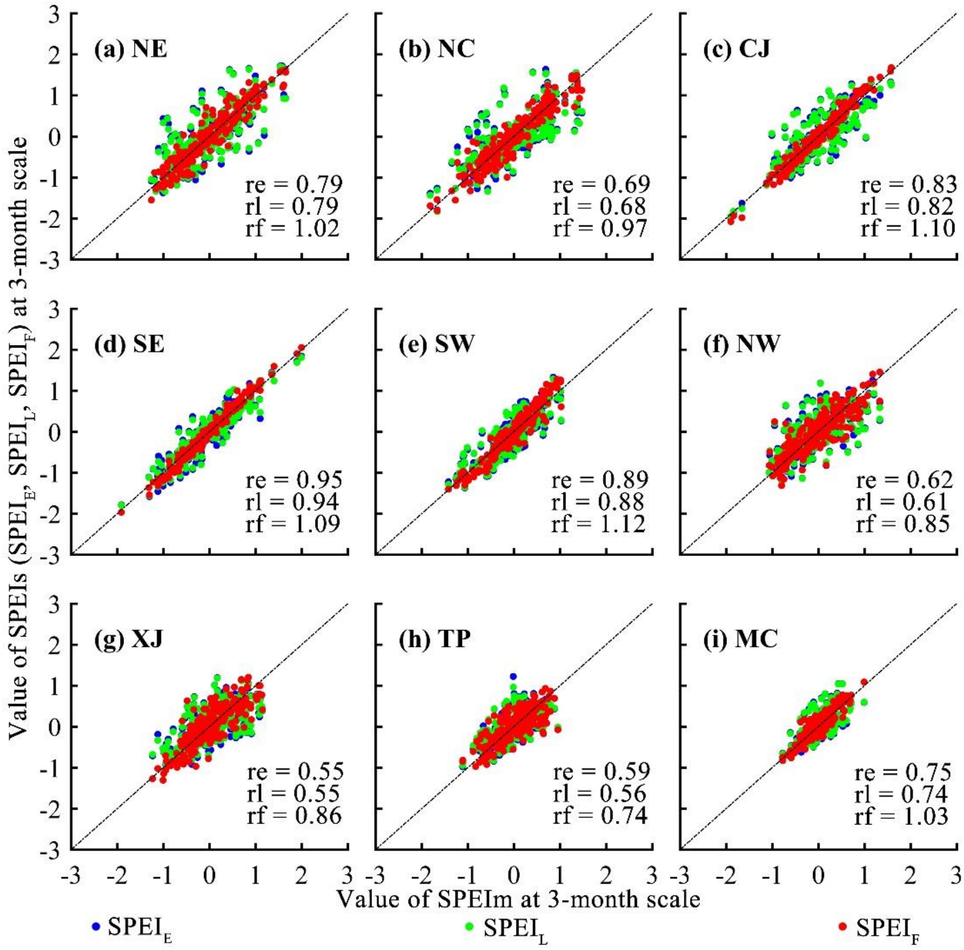

Fig. 8. The value of grid average SPEIs (SPEI$_E$, SPEI$_L$ and SPEI$_F$) vs SPEIm at 3-month timescale in eight regions and MC. re, rl and rf represent the slope of the linear fit between SPEI$_E$ against SPEIm, SPEI$_L$ against SPEIm and SPEI$_F$ against SPEIm, respectively.

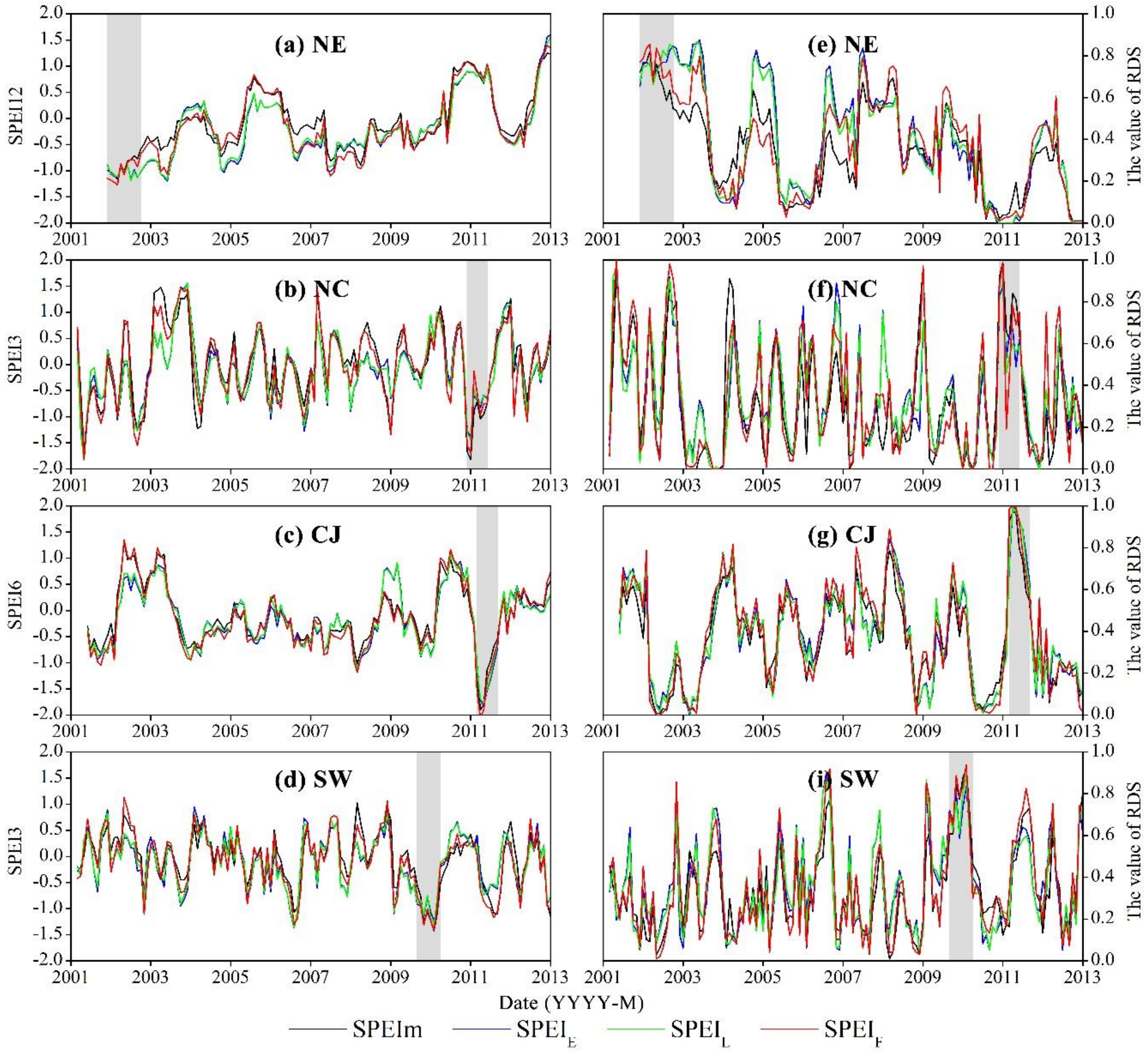

Fig. 9. Time series of grid average SPEI and RDS (ratio of drought stations) in NE, NC, CJ and SW, for which the specific start–end time and other information of the typical drought event as shown in Table 4.

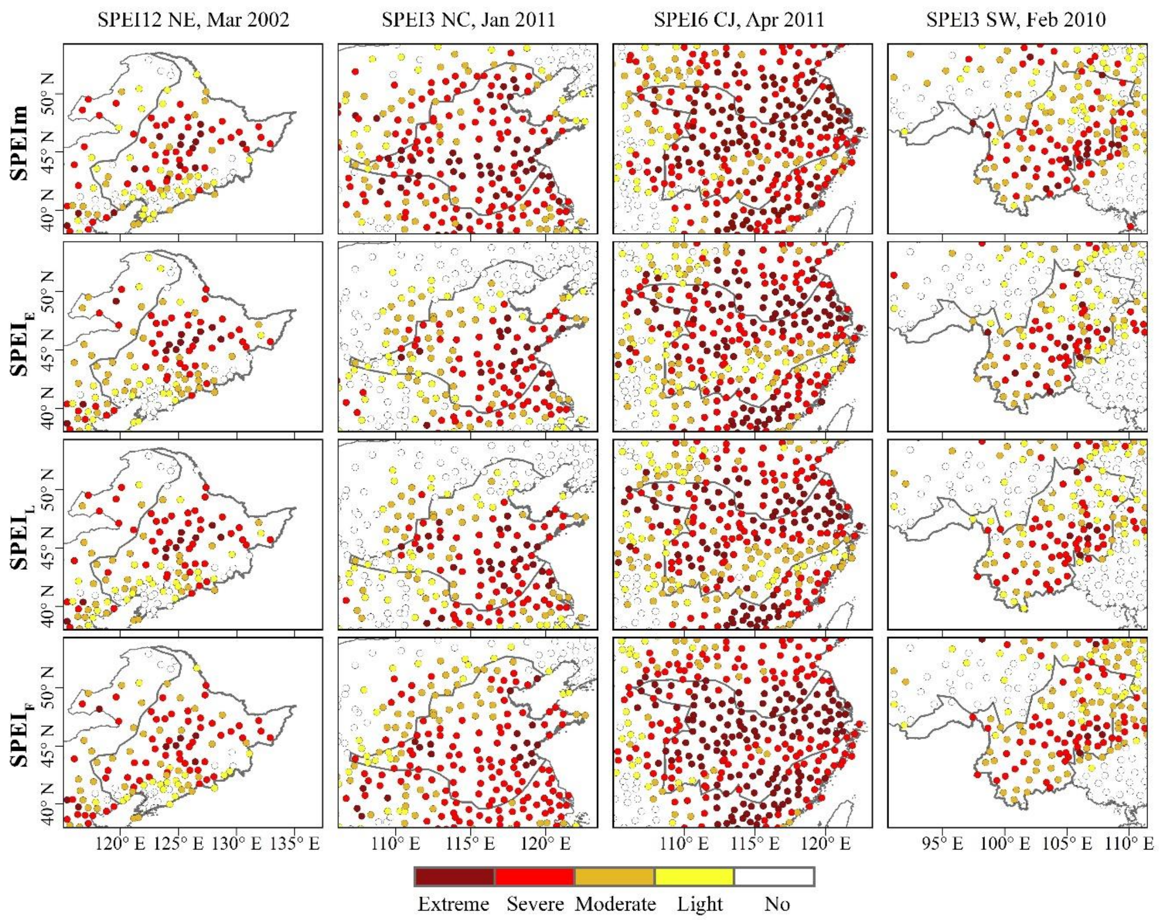

Fig. 10. Spatial distribution of monthly grid SPEIs ($SPEI_E$, $SPEI_L$, $SPEI_F$) versus SPEIm for drought events in NE, NC, CJ, and SW.